Undergraduate Honor Thesis Project

A study of a Ventricular Motion in Cardiac MRI using Deformable Models

Submitted to

The Engineering Honors Committee

119 Hitchcock Hall

College of Engineering

The Ohio State University

Columbus, Ohio 43210

By:

Toshihiro Okada

555 Ozem Gardner Way

Westerville, Ohio 43081

Advisor: Professor Kim. L Boyer, The Ohio State University

Date Presented: January 26, 2007

Date Received: January 26, 2007

Abstract

We experimented with a novel deformable model that track the right ventricle's (RV) wall motion through complete cardiac cycle by using a snake-like approach. The model uses a complex Fourier shape descriptor parameterization for efficient calculation of forces that constrains contour deformation. Even though the complexity exists in RV boundary shape, the model tracks the contour correctly and shows the robustness in weak contrast and noisy edge map. We also present a quantitative evaluation of delineation accuracy by comparing manual segmented contours and semi-automatically segmented contour, to check the reliability of our deformable model. The extracted shapes shows that the error between two contours to be an average of two pixels from 256 pixels by 256 pixels of cardiac magnetic resonance images. We used the spatio-temporal characterization of ventricular wall motion, obtained by our model, to help classifying the *Intra-ventricular dyssynchrony* (IVD) in the LV - i.e. asynchronous activation of LV wall - by adding RV information of ventricular movement to existing data. The classifying method was to use a popular statistical pattern recognition method of the Principal Component Analysis and the Fisher's Linear Discriminant Analysis. From a database contains 33 patients, our classifier produced correct classification performance of 87.9 % with the RV data, which shows the promising improved IVD classification as contrast to current criteria for selecting therapy, which provided the correct classification of just 84.8 % on the same database with only the LV data.

Table of Contents

List of Figures

Acknowledgement

I am very thankful to Professor Kim L. Boyer and Paulo F. U. Gotardo for great support on this project, Professor Bradley D Clymer and College of Engineering for this great opportunity. I am grateful for my father, Seiichiro, and mother, Emiko, for all the support for the school. I also appreciate Dijia Wu, Jun Kong, Sean Winfree, Ke Sun, and Chen Lianghao for great discussion on related subjects, and Christopher Begin for writing help

1. Introduction

Despite continuing advances in medical imaging technologies, such as magnetic resonance imaging (MRI), much work remains in automated analysis of the resulting data to maximize these impacts on patient care. In most diseases early detection as well as accurate classification helps reduce the risk and impact of the diseases. One of the more promising medical technologies is cardiac magnetic resonance imaging (CMRI).

CMRI provide comprehensive cardiovascular images of four-dimension (3D and time) without ionizing radiation and with high signal-to-noise ratio as compared to other cardiac diagnostic modalities [1]. Multi-slice multi-phase (MSMP) short-axis scanning, or four-dimension short-axis cine MRI, enables a detailed study of cardiac anatomy and its function during both at rest and stress conditions [1]. MSMP short-axis scanning routinely acquired data during clinical examinations comprising high-resolution throughout the cardiac cycle, on a number of parallel planes known as “slices,” through the human heart. However, due to large amount of image data generated during scanning, typically 200 – 300 images, analysis of cardiac structure and function can become a strenuous task. As a result, automatic segmentation methods have been investigated to reduce time. Yet, the automatic segmentation method has many problems. Such problems include the lack of standards, difficulty in defining segmentation, and the lack of standards in statistical analysis [1]. Moreover, automated analysis of cardiovascular MRI remains challenging due to its natural variability of structure, turbulent blood flows, or the interference of other cardiac structures. The presence of noise and other artifacts can also cause the image information to be incomplete, distorted, or unreliable. For these reasons, automated data/image analysis has become a very challenging problem, and many researches have been investigating and researching new techniques.

The main goal of this project is described in two parts. We first develop software to detect and track the cardiac wall motion of the right ventricle (RV) via a series of CMRI. The software is developed by using the techniques of novel deformable model with complex Fourier shape descriptor, introduced by Paulo F. U. Gotardo [1]. The manual segmentation program is also implemented and the results are compared in order to assure the accuracy of automated contour tracking. Then we make use of the result of our deformable model to provide data that may help classifying *the Intra-ventricular Dyssynchrony* (IVD) in the left ventricle (LV). IVD is one of symptoms that corresponds to the non-uniform activation of the ventricular walls. Dyssynchronous motion, simply the symptom, is mainly considered as asymmetric muscle hypertrophy, reduction in contractility, filling time, and ejection fraction [1]. Improved characterization of the symptom will aid physicians in determining the method of treatment. The treatment of the IVD, cardiac resynchronization therapy (CRT), has provided positive results in restoring ventricular function, and it can improve quality of life for some patients. CRT re-coordinates the beating of the two ventricles by pacing multiple sites in the ventricles [2]. However, CRT is very difficult to apply due to difficulty in characterization of dyssynchrony; the main clinical issue concerning CRT is the placement of the leads and the appropriate number. In this project, we formulated the detection of IVD using statistical pattern analysis [1]. Our deformable model obtains the contour data over complete cardiac cycle. Then, the results will be applied to the Principal Component Analysis (PCA) and the Fisher Linear Discriminant Analysis (LDA) to detect and characterize IVD.

In the next sections, we first discuss prior works, which are the general deformable model idea, the Active contour model, and the Fourier shape descriptor in the deformable model (section 2). We then discuss important parameters used in our deformable model (section 3), followed by our experimental results in extracting RV shapes and comparison between manual segmentation (section 4), and IVD detection (section 5). Conclusion remark and future work is discussed in section 6.

2. Related Work

There are several researches that have been done prior to this project being initiated, and they are very helpful in understanding the current problem as well possible improvements. In this section, the basic idea of the deformable model, the Active contour model, and the Fourier Descriptor will be further discussed.

2.1 Deformable model

Many automated analysis of CMRI have been investigated and developed [1], [3], [4], [5], [6], [7]. In computer vision and image analysis literature, applying high-level knowledge at some stage of the data analysis – for instance, integrating global shape characterization and local image evidence - has been investigated in order to reduce the complexity of problems. These techniques are well known in computer vision literature as *deformable models* [1]. The deformable model consists of variety of types, such as Active Shape Models (ASMs), Active Appearance Models (AAMs), and Active contour models (known as snake). These models have provided promising results because they can capture high-level knowledge from manually generated results, provided by experts, and accommodate variation in a way that characterizes the class of the object of interest [1]. However, in order to use these models, they require initial training data sets with manually generated results, which may be an even more strenuous task for the spatio-temporal model. On the other hand, in medical image analysis, model-based approaches (i.e. top-down) faced the problems of *natural structure* or *gold standard* [1]. For this reason, normal, healthy anatomical structure is required for inter-sample variations. Furthermore, observer's bias will be strongly reflected in the result that may introduce misleading information, which could mean the consistency of the result will be weak.

The fundamental idea of the deformable model techniques can be represented in a Bayesian formulation with the maximum *a-posteriori* (MAP) estimation or the maximum likelihood estimation (MLE). For the case of 2D contour or shapes described by a parameter vector θ from an image I. From Bayes rule,

$$P(\theta \mid I) = \frac{P(\theta)P(I \mid \theta)}{P(I)} = \alpha\, P(\theta)P(I \mid \theta) \qquad (1)$$

where $\alpha = P(I)^{-1}$ is a normalizing constant that ensure $P(\theta \mid I) \in [0,1]$. The goal of the model is to find the contour that maximizes the posterior $P(\theta|I)$. The MAP estimation is given by:

$$\hat{\theta} = \arg\max_{\theta}\{\ln P(\theta) + \ln P(I \mid \theta)\} \qquad (2)$$

where the first term, the parameter's vector or priori distribution, represents expected shape, and the second term is image evidence of each possible contour instance. Thus, by maximizing the sum of these two terms, one can represent maximizing the high-level domain information and low-level observation data, the goal of the deformable model. However, there exists a trade off between how well extracted contour match with general expectations and how well does it agrees with the specific image data or instance being considered.

2.2 Active Contour Model

The deformable model presented in this project uses cardiac contour for tracking, most likely the ventricular wall, through a complete cardiac cycle. The model follows snake-like approach but uses complex Fourier shape descriptors. This approach makes use of not only edge detection but also the texture around the evolving contour to design image forces that guide contours toward desired structures in the image. By integrating the texture information and edge information, the accuracy rate of the contour detection has been increased. Manual segmentation is required for the initial image of the MRI sequence with only a few points depending on the image (typically around 10-15 points), but no other training set is required. This model was originally designed by Paulo F. U. Gotardo, and his model is designed for tracking the left ventricle (LV). This deformable model requires less data samples than elliptical Fourier shape descriptor model, in addition to easier initial shape segmentation.

In order to understand this model, we first consider the deformable model under the energy minimization framework. The desired contour $\hat{\theta}$ is the minimum of the sum of three kinds of potential energies: external energy, internal energy, and image energy.

$$\hat{\theta} = \arg\min_{\theta}\{E_{external}(\theta) + E_{internal}(\theta) + E_{image}(\theta)\} \tag{3}$$

The internal and external energy, E_{internal} and E_{external}, acts as prior information (first term in Equation 2), and image energy, E_{image}, acts as the data evidence (second term in Equation 2). The models often consider these energies in corresponding *forces*, in which image force, F_{image}, tends to deform the image while both external and internal force, F_{external} and F_{internal}, constrain its deformation. These forces are found by the differentiation of energy, or the gradient of energy [8]. In order to minimize the energy, conjugate gradient decent is required to find the nearest minimum in an energy hypersurface as shown in Figure 1[8], and the final state of snake $\hat{\theta}$ is achieved when the forces are in balance [1]:

$$F_{internal}(\hat{\theta}) + F_{external}(\hat{\theta}) + F_{image}(\hat{\theta}) = 0 \tag{4}$$

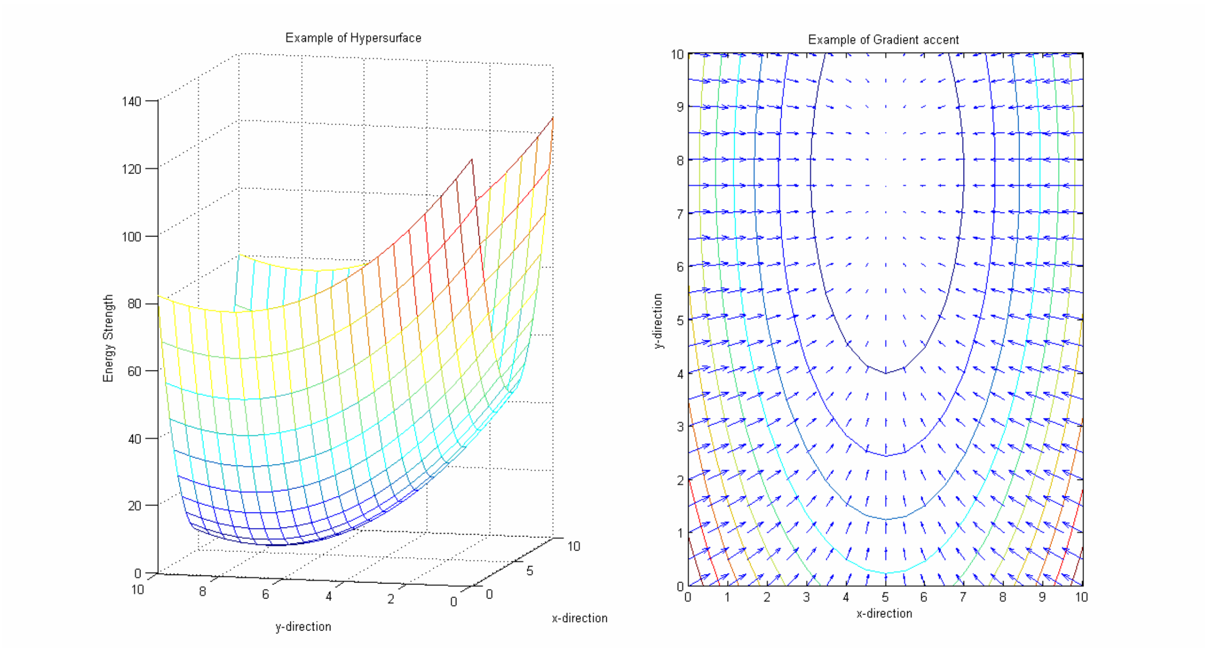

Figure 1: Graphical view of an example of Energy Hypersurface (left) and Gradient Decent optimization (right) showing how model deform to desired position as shown in equation (4).

2.3 Fourier shape descriptor

Fourier shape descriptor is a technique of tracing the contour to a desired location with a small number of parameters. The model is generated by many ellipses rotating in the same manner with different lengths. Staib and Duncan have modeled the deformable model by using the parametric Fourier descriptor [5]:

$$\begin{bmatrix} x(t) \\ y(t) \end{bmatrix} = \begin{bmatrix} a_0 \\ c_0 \end{bmatrix} + \sum_{k=1}^{N} \begin{bmatrix} a_k & b_k \\ c_k & d_k \end{bmatrix} \begin{bmatrix} \cos(kt) \\ \sin(kt) \end{bmatrix} \qquad (5)$$

where the value of α_0 and c_0 are the coordinates of the contour's centroid (DC component), and α_k, b_k, c_k, and d_k are the Fourier coefficients of the x(t) and y(t) with period of 2π, $t \in [0,2\pi)$:

$$\begin{aligned} a_k &= \frac{1}{\pi}\int_0^{2\pi} x(t)\cos(kt)dt, & b_k &= \frac{1}{\pi}\int_0^{2\pi} x(t)\sin(kt)dt \\ c_k &= \frac{1}{\pi}\int_0^{2\pi} y(t)\cos(kt)dt, & d_k &= \frac{1}{\pi}\int_0^{2\pi} y(t)\sin(kt)dt \end{aligned} \qquad (6)$$

For each k in the summation above (5), the corresponding matrix defines a rotated ellipse with a starting point position (phase shift). Thus, the contour described by these parameters, say $\theta = (a_0,$

$c_0, \ldots, a_k, b_k, c_k, d_k, \ldots)$, is represented as a combination of ellipses, with N corresponding to the number of ellipses used in the shapes. Figure 2 shows how the shapes are defined by the number of ellipses.

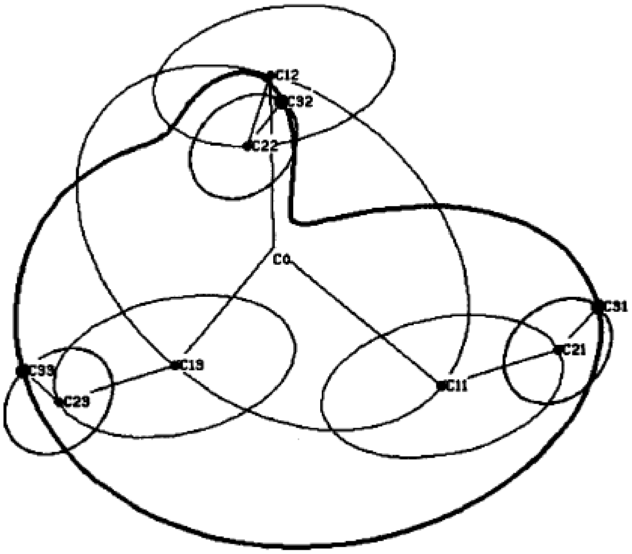

Figure 2: Elliptical Fourier shape descriptor example [5]

The number of the Fourier series coefficients, or ellipses, required is dependent on the complexity of the shape. Many structures found in medial images are typically characterized by smooth contours, for which the number of required ellipses is usually small (*e.g.* from five to ten).

Instead of the parametric Fourier coefficient, our model uses complex numbers to allow more efficient formulation of regularizing forces. Image analysis is often simplified by looking at the invariant properties of shape and, typically, normalizing the shape representation variable, such as scale, rotation, and starting point, may be necessary. In this case, complex Fourier descriptors provide simplified initialization. The representation of complex Fourier descriptor is

$$s(t)=x(t)+j\,y(t) = \sum_{k=-N}^{N} S_k e^{jkt} \tag{7}$$

where each complex number $S_k = \alpha_k + j\,\beta_k$, with $\alpha_k,\ \beta_k \in \Re$, is treated as a rotating phasor with magnitude $|S_k| = \sqrt{\alpha_k^2 + \beta_k^2}$ and phase angle $\phi_k = \tan^{-1}\left(\frac{\beta_k}{\alpha_k}\right)$. Frequency of the phasor determine the direction of the rotation in a complex plane; positive frequency (*k>0*) rotates counterclockwise and negative frequency (*k<0*) rotates clockwise. The frequency index *k* is the number of complete rotations, 360 degrees, performed by the corresponding phasor, and each pair of descriptor S_k and S_{-k} describes and ellipse [1]. Similarly to Staib and Duncan's parametric Fourier shape descriptor, by replacing S_k of Equation (7) by real parameter α_k and β_k, it can be shown as:

$$\begin{bmatrix} x(t) \\ y(t) \end{bmatrix} = \sum_{k=-N}^{N} \begin{bmatrix} \alpha_k & -\beta_k \\ \beta_k & \alpha_k \end{bmatrix} \begin{bmatrix} \cos(kt) \\ \sin(kt) \end{bmatrix} = \begin{bmatrix} \alpha_0 \\ \beta_0 \end{bmatrix} + \sum_{\substack{k=-N \\ k\neq 0}}^{N} \begin{bmatrix} \alpha_k & -\beta_k \\ \beta_k & \alpha_k \end{bmatrix} \begin{bmatrix} \cos(kt) \\ \sin(kt) \end{bmatrix} \tag{8}$$

this, in fact, can replace Staib and Duncan's parameterization, from Equation (5), as:

$$\begin{bmatrix} a_k & b_k \\ c_k & d_k \end{bmatrix} = \begin{bmatrix} \alpha_k + \alpha_{-k} & -\beta_k - \beta_{-k} \\ \beta_k + \beta_{-k} & \alpha_k - \alpha_{-k} \end{bmatrix} \tag{9}$$

For each hypothetical contour θ, Staib and Duncan considered a corresponding template image τ_θ as having ones along the contour and zeros elsewhere. They then consider matching θ and τ_θ using Bayes rule with MAP estimation (Equation (2) and (3)), with conditional term, $lnP(I|\theta)$, which approximates, by a correlation between template image τ_θ and edge strength, the value of image I_e [5]. This corresponds to integrating edge strength value along the contour. By assuming a priori parameter θ_i as independently distributed Gaussian parameter, $\theta_i \sim N(\mu_{i,} \sigma_i^2)$, the estimated contour $\hat{\theta}$ is one maximizing the following equation [1]:

$$f(\theta) = -\sum_{i=1}^{2+4N} \frac{(\theta_i - \mu_i)^2}{2\sigma_i^2} + \int_0^{2\pi} I_e \,|_{(x(t;\theta),y(t;\theta))}\, dt = -\sum_{i=1}^{2+4N} \frac{(\theta_i - \mu_i)^2}{2\sigma_i^2} + \int_0^{2\pi} I_e \,|_{s(t;\theta)}\, dt \tag{10}$$

The contour $\hat{\theta}$ is found from a user supplied initial contour by performing gradient accent optimization, also known as steepest-ascent hill climbing [1], which gradient vector $\nabla f(\bullet)$ from Equation (10) is given by:

$$\begin{bmatrix} \vdots \\ \frac{\partial f}{\partial \theta_i} \\ \vdots \end{bmatrix} = -\begin{bmatrix} \vdots \\ \frac{\theta_i - \mu_i}{\sigma_i^2} \\ \vdots \end{bmatrix} + \int_0^{2\pi} \frac{\partial I_e}{\partial x}\Big|_{x(t;\theta)} \begin{bmatrix} \vdots \\ \frac{\partial x(t;\theta)}{\partial \theta_i} \\ \vdots \end{bmatrix} + \frac{\partial I_e}{\partial y}\Big|_{y(t;\theta)} \begin{bmatrix} \vdots \\ \frac{\partial y(t;\theta)}{\partial \theta_i} \\ \vdots \end{bmatrix} dt \qquad (11)$$

The parameter of the right hand side of the equation above can be thought of as the following; the first vector is considered as an external force, and integrand's partial derivatives are considered as an image force. There also exist additional constraints imposed by the model which are considered as an internal force. The parameter of this deformable model is further investigated in following section.

3. Complex Fourier Descriptor snake modeling

In the previous section, we discussed the integrating complex Fourier shape descriptor into the snake-like deformable model. In this section, we will discuss further into this deformable model fitting process: image forces, external forces, and internal forces.

3.1 Image Force

Metaphorical image forces are a very important parameter, which are responsible for deforming the initial contour to the desired boundary location. Typically, these 2D force vectors are defined by the edge information and texture information of the image. In order to find this information, we must first compute the magnitude of image's brightness gradient, $I_e = |\nabla I|$, and then take x- and y-derivative of the contour from finite difference. Also, there are no forces acting on the contour in the interior of homogeneous region, where I_e is negligible [1]. As a result, precise initial contour close to the desired boundary is necessary.

The edge information is very important to deforming the contours; however, it is very difficult to interpret and detect the correct edge. If an edge map is initially available, it is possible to assign force vectors to each pixel relative to the closest edge to create a slope inside of non-edge pixels [1]. Then those forces with inverted signs move the contour towards the edge like gradient decent optimization of hypersurface explained in section 2. The study suggests scaling the force vector to unit-length in order to avoid the large "jump" of the contour, which may lead the contour to deform to a different edge. To identify the image forces acting on the contour, a number of equally spaced points $t_i \in [0, 2\pi]$ with $1 \le i \le L$, are sampled from the contour parameterization, with contour length L is computed as [1]:

$$L^2 = 4\pi^2 \sum_{k=-N}^{N} k^2 |S_k| = 4\pi^2 \sum_{k=-N}^{N} k^2 \left(a_k^2 + b_k^2\right) \tag{12}$$

Then by recalling Equation (11), the resulting edge-based image forces acting on a contour with descriptor vector ***S*** are explained [1]:

$$F_{image}(S) = \sum_{i=1}^{L} \left[I_x\big(x(t_i;S), y(t_i;S)\big)\nabla x(t_i;S) + I_y\big(x(t_i;S), y(t_i;S)\big)\nabla y(t_i;S) \right] \tag{13}$$

where I_x and I_y are the two components of the image force vector and gradient vector are expressed and each component is computed from Equation (8) as [1]:

$$\nabla x(s(t_i;S)) = \begin{bmatrix} \vdots \\ \dfrac{\partial x(t_i;S)}{\partial a_k} + j\dfrac{\partial x(t_i;S)}{\partial b_k} \\ \vdots \end{bmatrix} = \begin{bmatrix} \vdots \\ \cos(kt) + j\sin(kt) \\ \vdots \end{bmatrix}, \quad k = -N, \ldots, N \tag{14}$$

$$\nabla y(s(t_i;S)) = \begin{bmatrix} \vdots \\ \dfrac{\partial y(t_i;S)}{\partial a_k} + j\dfrac{\partial y(t_i;S)}{\partial b_k} \\ \vdots \end{bmatrix} = \begin{bmatrix} \vdots \\ \sin(kt) + j\cos(kt) \\ \vdots \end{bmatrix}, \quad k = -N, \ldots, N \tag{15}$$

The above equation will determine the edge-based image force; however, since we want to perform tracking over the sequence of images, I_n with $n \in \{1,2,\ldots,20\}$ (CMRI generates 20 images per slice), we can expect that the boundary shape and gray level pattern near the contour shouldn't change dramatically. Thus, keeping the texture information around the contour helps the consistency of the image texture or vicinity of the contour [1]. With this texture-based image forces, the model is able to deform with the weak edge information.

In order to obtain the vicinity information of the contour from the final shape obtained previously I_{n-1}, we sample W_0 pixel values along the normal direction of the contour [1]:

$$s_{\perp}(t)=\begin{bmatrix} u(t) \\ v(t) \end{bmatrix}=\sum_{k=-N}^{N} k\begin{bmatrix} a_k & -b_k \\ b_k & a_k \end{bmatrix}\begin{bmatrix} \cos(kt) \\ \sin(kt) \end{bmatrix} \tag{16}$$

at a number of locations similar to contour sampling of Equation (12). This texture-based force helps to determine the direction of the deformation by simply adding $sign(p_i)\frac{s_{\perp}(t_i)}{\left\| s_{\perp}(t_i) \right\|}$ to the edge-based image force [1]: where p_i is the position of the best match obtained from comparing the current image texture and previous image texture.

These image forces ensure that the deformable model tracks the desired contours. Thus, the initialization is important to receive high-level knowledge on not only texture, but also on the expected shape for subsequent images.

3.2 External Force

In many applications of the deformable model, the prior knowledge of the desired model should be integrated with the additional constraints on the contour's deformation in order to achieve successful tracking. For the case of non-rigid object tracking over a CMRI sequence, data evidence may be missing or corrupted by noises or other image artifacts. However, as we mentioned in the previous section, the subsequent images in CMRI are so "similar" to the contour extracted from previous image I_{n-1},

$$S_k^{(n-1)}=a_k^{(n-1)}+jb_k^{(n-1)},\ k=-N,\dots,N \tag{17}$$

that it can be used to help deform the contour correctly. By introducing the *external forces*, which is the bias toward an expected shape by considering prior parameter distribution or strong image evidence, the deformable model can be able to reduce the number of false positives. Similar to Staib and Duncan's approach [5], we assume the Fourier descriptor as independent Gaussian random variable with *scale-normalized* Fourier descriptors, $\frac{S_k}{|S_1|}$, for prior distribution [1]:

$$\alpha_k^{(n)} = \frac{\alpha_k^{(n)}}{\left|S_1^{(n)}\right|} \sim N\left(\alpha_k^{(n-1)}, \frac{\sigma^2}{|k|}\right), \qquad k \notin \{0,1\} \tag{18}$$

$$\beta_k^{(n)} = \frac{\beta_k^{(n)}}{\left|S_1^{(n)}\right|} \sim N\left(\beta_k^{(n-1)}, \frac{\sigma^2}{|k|}\right), \qquad k \notin \{0,1\} \tag{19}$$

with user-defined variance, σ^2. By maximizing the log likelihood of the descriptors $\alpha^{(n)}$ and $\beta^{(n)}$ from the given initial descriptor $S^{(n-1)}$, in other word find the maximum correlation [1]:

$$\ln P\left(\alpha^{(n)}, \beta^{(n)} \mid S^{(n-1)}\right) = -\sum_{\substack{k=-N \\ k\neq 0,1}}^{N} \frac{|k|}{2\sigma^2}\left(\alpha^{(n)} - \alpha^{(n-1)}\right)^2 - \sum_{\substack{k=-N \\ k\neq 0,1}}^{N} \frac{|k|}{2\sigma^2}\left(\beta^{(n)} - \beta^{(n-1)}\right)^2 \tag{20}$$

Also, the External force is given by the gradient vector with each component expressed as [1]:

$$F_{external}(S) = \nabla \ln P = \begin{bmatrix} \vdots \\ \frac{\partial \ln P}{\partial \alpha_k} + j\frac{\partial \ln P}{\partial \beta_k} \\ \vdots \end{bmatrix}, \qquad k = -N, \ldots, N \tag{21}$$

where:

$$\frac{\partial \ln P}{\partial \alpha_k} = -\frac{|k|}{\sigma^2}\frac{\left(\alpha_k^{(n)} - \alpha_k^{(n-1)}\right)}{|S_1|} \tag{22}$$

$$\frac{\partial \ln P}{\partial \beta_k} = -\frac{|k|}{\sigma^2}\frac{\left(\beta_k^{(n)} - \beta_k^{(n-1)}\right)}{|S_1|} \tag{23}$$

The strength of the external force can be controlled by changing the user-defined variance, σ^2.

3.3 Internal Force

Even though the Fourier series parameterization of the deformable model comprises smoothness constraints, the model can still generate sharp corners as well as contour crossing themselves. This can be solved by introducing additional internal force which takes account of more constraints from the contour's curvature derivative. This, however, makes deformation or gradient ascent computation much more complex. In order to resolve the problem, we define an additional internal (tension) force that does not involve a gradient ascent computation. These forces are designed to be weaker than image forces, which ensure the contour will be allowed to deform under the influence of image forces.

The function of this internal force is to minimize the contour's length, which is analytically computed using approximation of the squared length L^2 of the contour given in Equation (12). Normalizing the contour is necessary to make the internal force to be independent of contour scale. Thus, we consider the descriptor vector as $\frac{S}{|S_1|}$ in computing L^2. Then, the internal force at a given point of the contour deformation process is given by:

$$F_{internal}(S) = -\nabla\left(L^2\right) = -\begin{bmatrix} \vdots \\ \frac{\partial\left(L^2\right)}{\partial\alpha_k} + j\frac{\partial\left(L^2\right)}{\partial\beta_k} \\ \vdots \end{bmatrix}, \qquad k = -N,\ldots,N \tag{24}$$

where:

$$\frac{\partial\left(L^2\right)}{\partial\alpha_k} = 8\pi^2 \frac{k^2\alpha_k}{\alpha_1^2 + \beta_1^2}, k \neq 0,1 \tag{25}$$

$$\frac{\partial\left(L^2\right)}{\partial\beta_k} = 8\pi^2 \frac{k^2\beta_k}{\alpha_1^2 + \beta_1^2}, k \neq 0,1 \tag{26}$$

$$\frac{\partial\left(L^2\right)}{\partial\alpha_1} = 8\pi^2 \frac{-\alpha_1}{\alpha_1^2 + \beta_1^2} \sum_{k\notin\{0,1\}} k^2\left(\alpha_k^2 + \beta_k^2\right) \tag{27}$$

$$\frac{\partial\left(L^2\right)}{\partial\beta_1}=8\pi^2\frac{-\beta_1}{\alpha_1^2+\beta_1^2}\sum_{k\notin\{0,1\}}k^2\left(\alpha_k^2+\beta_k^2\right) \tag{28}$$

Since the constant $8\pi^2$ is found in all terms, we can simply drop the value to make the resulting internal force to be relatively weaker than the image forces.

3.4 Deformable model with complex Fourier Descriptor

The input CMRI data for each patient corresponds to one slice of the MSMP data over a complete cardiac cycle. The first image of this sequence of 20 images is assumed to be a fully expanded ventricle, or the end of diastole, which often clearly distinguishes the boundaries that allows us to easily obtain proper initialization. As we discussed in the previous section, our deformable model requires the precise initialization to correctly tracking the contour. This user-supplied contour is then used to initialize tracking in the subsequent images as follows:

Given the CMRI data and the initial shape descriptor ***S*** with corresponding reference texture vector $s_\perp(t_i)$, our objective is to maximize the contour's likelihood function, denoted *f(**S**),* from Equations (2)-(4) [1]. During the contour evaluation, the gradient of $f(\bullet)$ corresponds to the deformable force acting on ***S***, obtained from Equation (13), (21), (24):

$$\nabla f(S)=F_{internal}(S)+F_{external}(S)+F_{image}(S) \tag{29}$$

We iteratively update ***S*** as

$$S=S+\gamma\ \nabla f(S) \tag{30}$$

until the magnitude of $\nabla f(S)$ is negligible, or the balance of force is reached, with γ to be a small constant giving the size of each step in the direction of the gradient [1]. The final shape ***S*** and the new set of reference texture are used to initialize the process of the next image.

In our model, tracking is performed in two directions in the periodic time sequence. The directions of the tracking are forward (consecutive image) and backward (previous image), and each track can be considered as a complementary subsequence of the cardiac cycle. The image indexes used in each subsequence are *n=1, 2, ..., 10,* for forward direction and *n = 20, 19, ..., 6,* for backward direction. This complementary subsequence of the deformation seeks the best merging point $n \in [6,10]$ by finding the minimum distance between the magnitudes of complex Fourier descriptors [1]. In this way the model not only reduces propagation error, but also increases the use of the user-provided initialization (manual) data. Since we define the initial image of the sequence at end of the diastole, the fully expanded ventricle, both directions of the track most likely see the contracting of the contour. As a result, it minimizes the errors that may occur during expansion.

4. Extraction and tracking of RV boundaries

In this section, we first discuss our deformable model techniques and present the results when applied to extract and track the RV boundaries. Then, we address the importance of manual segmentation followed by comparison of the data between our deformable model and manual segmentation. This section illustrates the method of comparing the resulting contour with manual segmentation. In order to determine the accuracy of the contour tracking, manual segmentation should be *conducted* by an imaging cardiologist. Therefore, the manual delineations, used here, only serve to illustrate the evaluation process.

4.1 Extraction and tracking of RV boundaries using deformable model

The deformable model presented by Gotardo [1], discussed in previous section, is specifically designed for tracking the LV contours. The RV contours, however, has different shape and surrounding textures as compared to the LV. As a result, there exists the difficulty in tracking of the RV contour accurately, by using the same model for tracking the LV. However, it is found to be that an appropriate modification of the deformable model allows tracking of the RV contour accurately.

The problems of tracking the RV, using the existing model for the LV, is because 1) the RV has a more complex shape than the LV, 2) part of the ventricular wall is sometimes too thin to be recognized by the deformable model, 3) there exist several false edges that may confuse the model in attempting to detect the correct contour, 4) irregularity of motion may be found in RV, and 5) RV sometimes does not appear clearly in the CMRI. Each problem has been carefully considered and modified appropriate parameters of the model with several experiments for each modification.

We have found that the problem (1), the complexity in the RV shape, can be solved by increasing the number of the ellipses used, problem (2)-(4) can be solved by modifying the force components in Equation (29) by simply multiplying each component by some constants α. The problem (5), on the other hand, is not a problem due to the deformable model. Though, changing the contrast of the image may be helpful to see the boundary. After several experiments, six ellipses, $N=6$ or thirteen Fourier coefficients, and about twelve to fifteen initialization points are found to be a reasonable number to shape the RV. Also, following modification found to decrease the error of deforming contour incorrectly as well as obtain the accurate initial segmentation:

- Reduced the tension force to comprise the irregular motion of the RV, or reducing the rigidity of the contour by multiplying $\alpha_{internal}$.
- Reduced the edge-based image force to decrease the dependency of the edge information, or increase the texture dependency of the model α_{edge}.

We have found $\alpha_{internal}$ to be 0.8 and α_{edge} to be 0.6 give the reasonable tracking result, and Figure 3 and Figure 4 shows the result of extracting and tracking the RV boundary for a normal and a dyssynchronous heart, respectively. Also, overlay of shapes during systole and diastole are shown with the arrow indicating the direction of contraction or extraction.

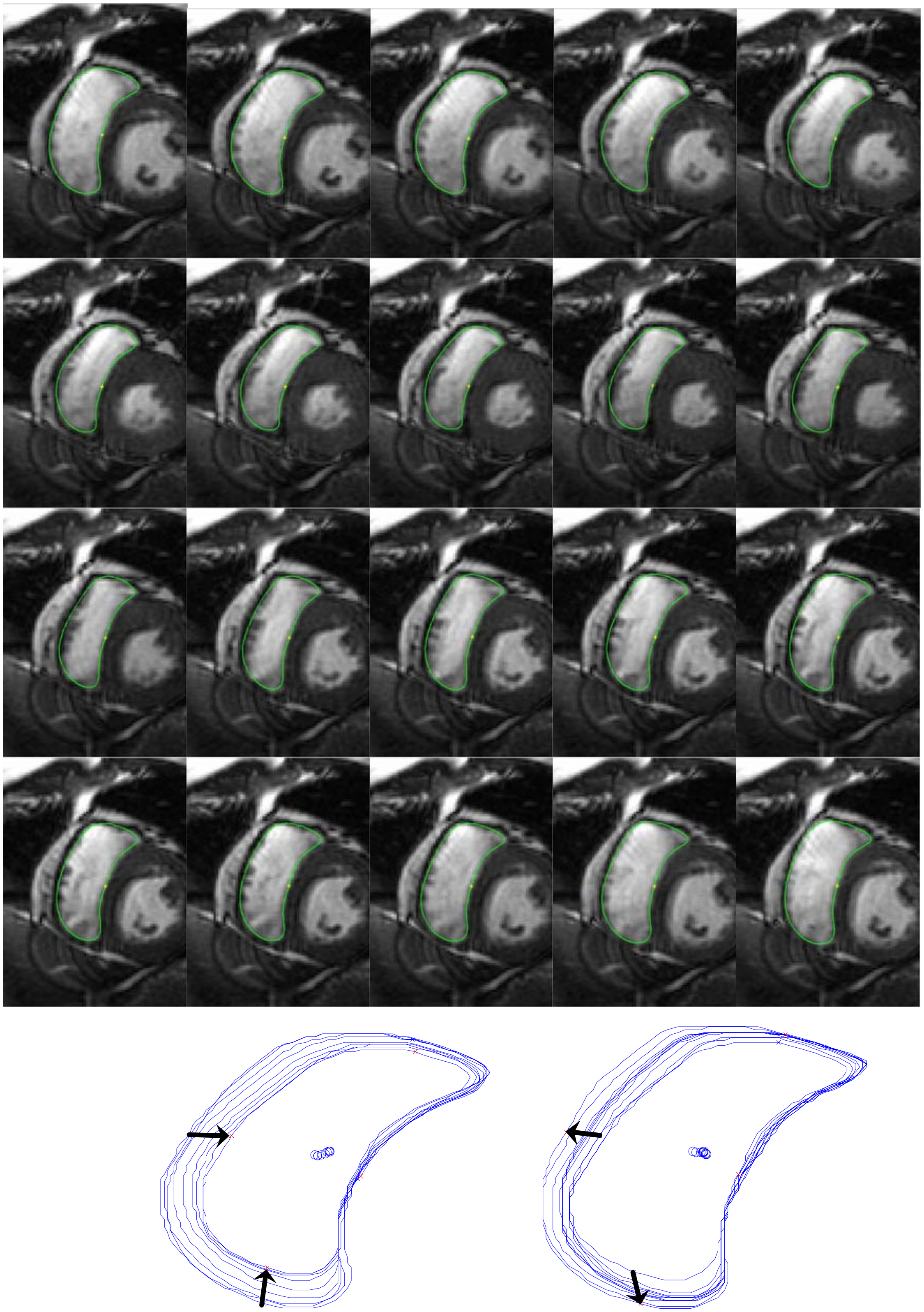

Figure 3: Extracting and tracking of RV without Dyssynchrony (top), Overlay image during systole (left) during diastole (right)

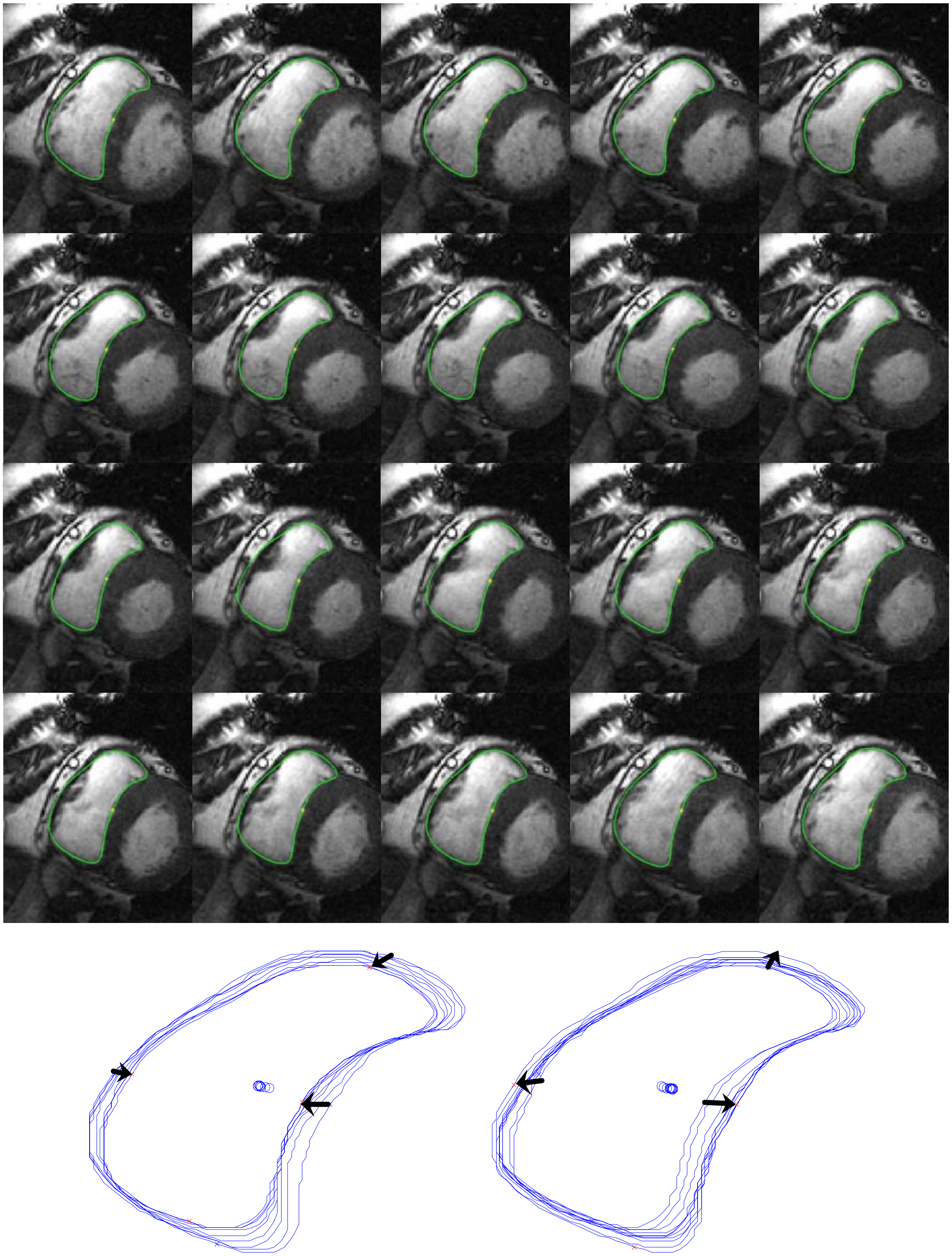

Figure 4: Extracting and tracking of RV with Dyssynchrony (top), Overlay image during systole (left) during diastole (right)

4.2 Manual Segmentation and Comparison of Contours

In order to insure that our deformable model be successful in tracking the desired contour, it is necessary to find the contour manually and compare the data obtained from manual segmentation and from our deformable model. Manual segmentation can be done with the use of a software tool to help delineate the RV into all the images of the sequence and store the resulting vector. Figure 5 shows the example of a visual comparison found in our deformable model from manually segmented contour.

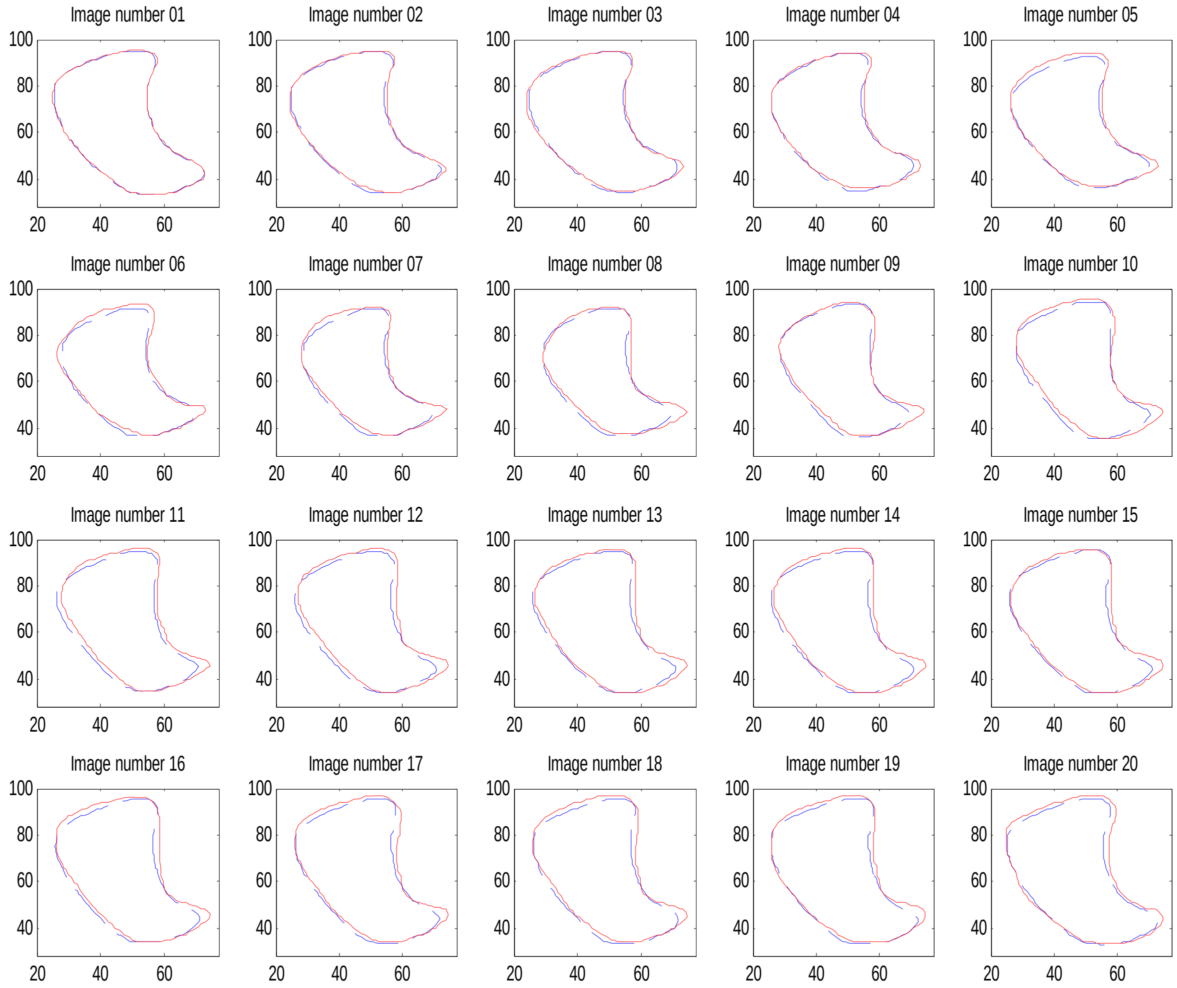

Figure 5: Contour obtained from semi-automated segmentation (Blue dashed line) Manual Segmentation (Red solid line)

One of the comparison methods is to find the spatial Euclidean distance between two contours. In this method, the Fourier descriptor vector ***S*** will be converted to spatial points, x and y using contour approximation described in Equation (8), and find the minimum distance from each point on the contours. However, the points will not be generated evenly in space from ***S***-matrix conversion, even though the points are generated evenly in time domain. That is, the descriptor tends to generate more points at the high curvature region of the contour. This problem can be solved by applying one of the two different methods described below:

Method 1:

- From Fourier parameter ***S***, finely sample the contour in spatial domain by using Equation (8)
- Apply memoryless scalar uniform quantization to the sampled contour
- Interpolate the larger gap in the quantized points
- Eliminate smaller gap in the quantized points

Method 2:

- Finely sample the contour in spatial domain similar to method 1
- Round points to nearest pixel, and eliminate duplicates

In method 1, memoryless scalar uniform quantization is considered as aligning the sampled contour onto fine grid space $Q_{x,y}$ and place points to nearest grid on the space, where x and y are called quantizer indices. The gap between the points in the quantized space is considered as the vertical and horizontal separation of the grids. The method 1 can be considered as applying method 2 with finer grid system.

The difference in quantizer indices between consecutive points will be separated evenly, with average difference of 1.7 indices, by the interpolation and the elimination process. These processes also reduced the number of points on a contour. Difference in quantizer indices before and after the process is shown in Figure 6 and Figure 7 below.

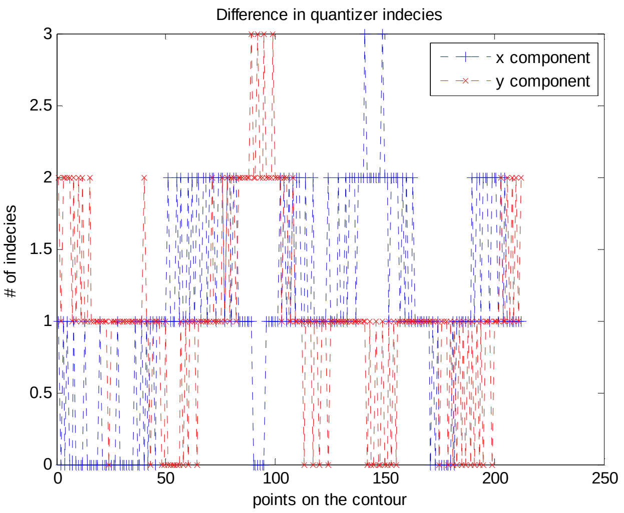

Figure 6: Difference in quantizer indices before interpolation and elimination

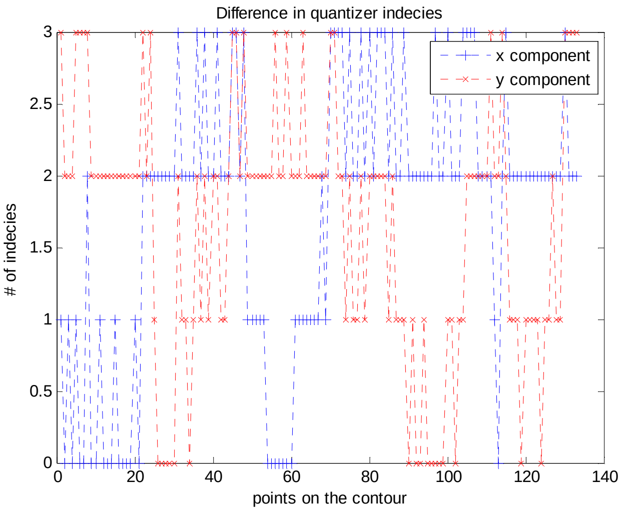

Figure 7: Difference in quantizer indices after interpolation and elimination

Two methods have been simulated and compared for several image sequences. As a result, method 1 gives better results without changing the contour information, as shown in Figure 8. Furthermore, by storing the quantizer indices, method 1 allows for faster calculation finding of Euclidian distance of the spatial data points. For instance, close point(s) can be easily found without calculating the actual Euclidean distance by searching quantizer indices around the point.

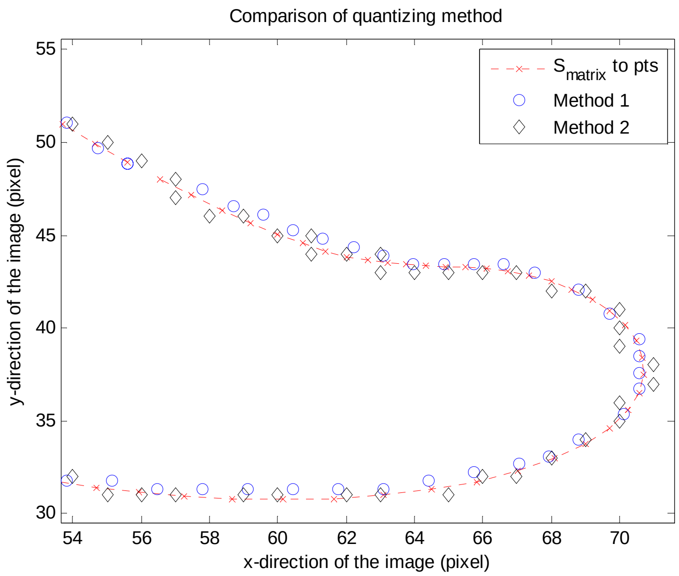

Figure 8: Comparison of method of quantization

Then, the Euclidean distance between two contours (error) will be calculated by finding the closest point pair from two contours. The closest pair can be easily found by using the quantizer indices obtained by method 1. Figure 9 shows the median, mean, and maximum error distance for each image in one of the sequences.

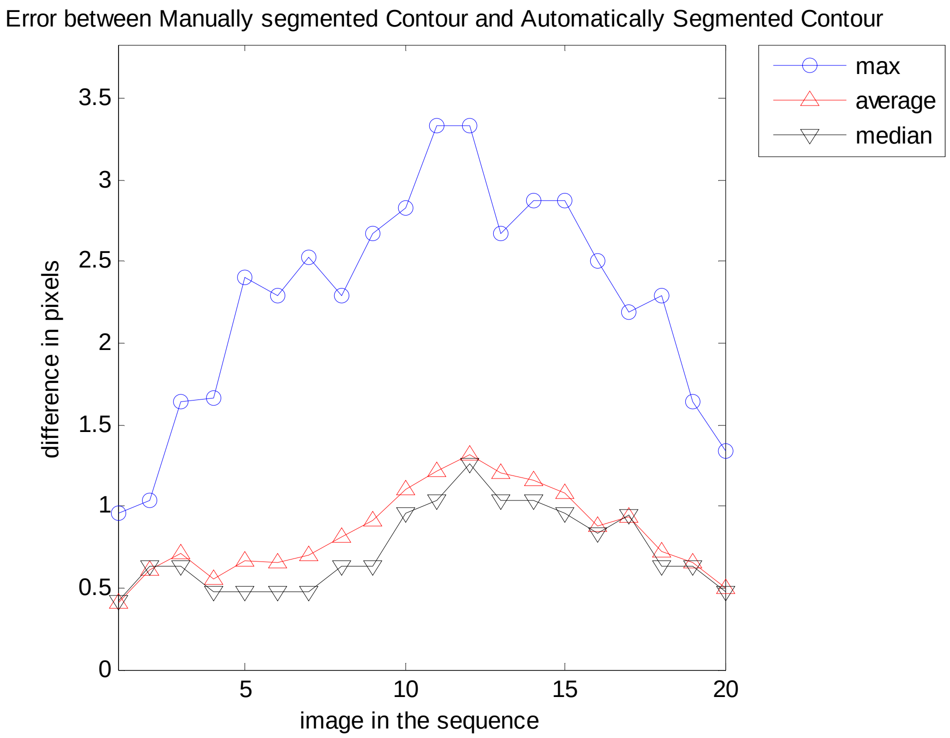

Figure 9: Error between manually segmented contour and automatically segmented contour

4.3 Experimental Result

The database of two methods of segmentations of 30 studies is compared in our experiments. The analysis of the results illustrates the accuracy of our deformable model, by finding and applying the elemental statistical analysis, which is to find either: 1) the minimum, 1st percentile, median, 3rd percentile, and maximum, or 2) mean, and standard deviation. We employ both methods to see the error distributions of each image as shown in Figure 10.

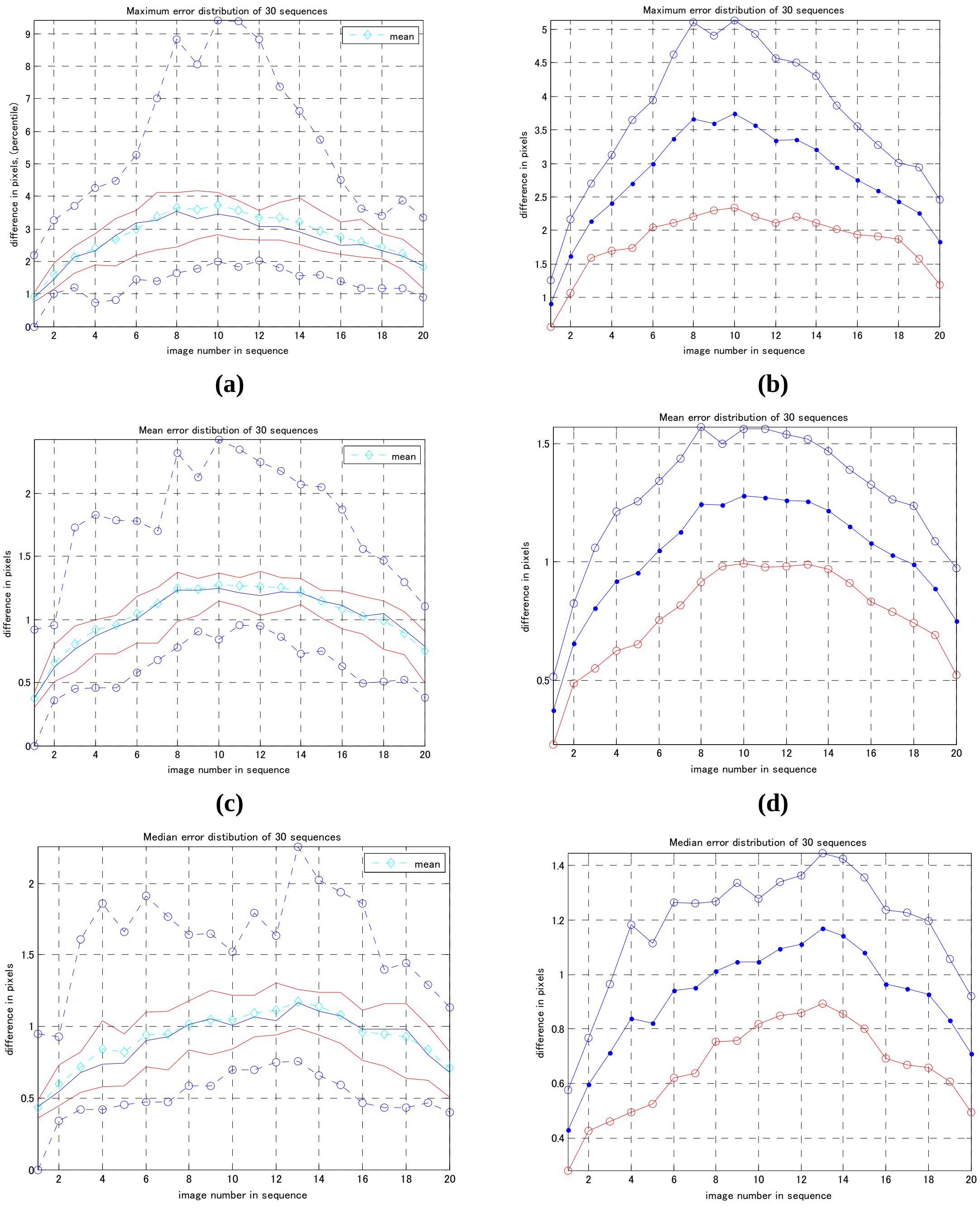

(a) **(b)**

(c) **(d)**

(e) **(f)**

Figure 10: Maximum Error distribution found by using (a) method 1 (b) method b, Mean Error distribution found by using (c) method 1 (d) method 2, Median Error distribution found by using (e) method 1 (f) method 2

The graphs of error distribution, obtained by using method 1, show the mean, minimum, 1st percentile, median, 3rd percentile, and the maximum error of the database. The graphs of error distribution, obtained by using method 2, show the mean error and standard deviation of error of the database. It can be found that errors tend to increase as the image number merged to the middle of the sequence, as expected. However, most of the errors between contours are confined within only 2 pixels, which are considerably small since the CMRI produces the image with dimension of 256 pixels by 256 pixels.

5. Dyssynchrony Detection

The detection of the IVD, in this project, was considered as statistical pattern recognition. We employed the techniques of statistical pattern recognition to detect the IVD as well as classify the RV for two classes, dyssynchronous or non-dyssynchronous. We began by performing statistical analysis by learning a classifier for two classes of RV from a number of training samples, each one describing the contraction and expansion of the RV during the complete cardiac cycle for two classes. The classifier is designed by using the Principal Component Analysis (PCA) and Fisher’s Linear Discriminant Analysis (LDA). Furthermore, since the CMRI sequences in our database depict RV in varying scale, starting position, and rotation, the normalization of the descriptor must be taken into account in order to increase the correction rate of classification of the classifier. In this section, we first discuss our classifier design including the normalization of Fourier descriptor, followed by the experimental result.

5.1 Classifier Design

The shape of RV is described by thirteen phasors, or six ellipses with a centroid, and for each sequence of CMRI, it provides 20 * 13 = 260 complex descriptors in spatio-temporal shape space. To design a classifier from this high-level shape space, the statistical pattern recognition techniques are applied to seek the “important” information. Such information describes the best representation of the data or best discriminate between two different classes. In order to make the information consistent in all sequences, normalization of Fourier descriptors is often performed in shape matching application to provide invariance of translation, scaling, rotation, and the contour's starting point [1]. The pattern recognition techniques are then applied when the shape space is consistent in all sequences of the database. This technique extracts the features from the shape space that determines low-dimensional feature space, which best represents the data or best discriminate between two different classes.

In many case, the normalization process of the shape descriptor discards the centroid information. However, we believe that translation of the centroid may contain useful information in determining the IVD. Here, instead of discarding the centroid, we preserve the centroid information by subtracting the initial centroid displacement from all other centroids in the cycle. This preserves relative displacement of other shapes with respect to initial shape, which can be neglected at any time. Also, to match a single shape, scale invariance is obtained by dividing the descriptors by the largest magnitude of the phasor: which, in our case, is the first positive component of the first shape $|S_1| = \sqrt{\alpha_1^2 + \beta_1^2}$, since we assumed that the initial image is at the end of diastole, fully expanded shape.

The statistical pattern recognition system operates in two modes: training and testing. In testing mode, the classifier learns the features for different classes of extracted low-dimensional feature space that best *represents* the data or best *discriminates* between different classes. Testing mode classifies the data by using the criterion acquired during training. The statistic pattern recognition techniques we employ in our classifier are PCA and LDA. PCA is a well-established technique for dimensional reduction that finds a compact representation for a data set by capturing the most representative feature subspace from the projection of the shape space without much loss of information [1], [6]. This is done by fitting the multidimensional Gaussian distribution, typically considered as hyperellipsoid, which the distribution is completely determined by the mean vectors of the sample and the sample covariance matrix. The extracted features, also known as the principal components, are determined by the eigenvalues of the covariance matrix, and are the vectors defining the larges axes of the hyperellipsoid. The resulting projection matrix has a column vectors of the first few eigenvectors associated with the largest eigenvalues:

$$M_{finalshape} = \lambda \times \mathrm{A} \tag{31}$$

where M is the projection matrix, or final shape matrix, λ is the eigenvectors of the principal component, and A is the mean-adjust data [6]. The reduction of the shape space is done by the PCA. However, PCA is an unsupervised technique that does not include the label information of the data [10]. In order to employ the label information, in addition to reduction in dimension, a common approach is the LDA. LDA is a technique that not only reduces the dimensionality of the space, but also maximizes the Euclidian distance between different classes while minimizing the distance within the same class [1]. The LDA is considered to maximize the following objective:

$$J(M) = \frac{M^T S_B M}{M^T S_W M} \tag{32}$$

where S_B is called between-class scatter matrix and S_W is called within-class scatter matrix with:

$$S_B = \sum_c N_c (\mu_c - \bar{x})(\mu_c - \bar{x})^T \tag{33}$$

$$S_W = \sum_c \sum_{i \in c} (x_i - \mu_c)(x_i - \mu_c)^T \tag{34}$$

where $\bar{x}$ is the mean of the vector x and μ_c is the mean of the vector within the class, and C is the number of classes [10]. The resulting projection matrix has its columns as leading eigenvectors of matrix $S_W^{-1} S_B$ with at most C-1 non-zero eigenvalues [1].

In order to find the best discriminates, components between classes from large vector space usually take a long time and are inefficient. It is common to apply PCA before LDA to reduce the dimensionality of the vector space before discriminating the classes. This method is referred to as PCA+LDA, and is one we employ in our training classifier. The testing is performed by fist projecting a normalized test sample onto the low-dimensional classification space obtained previously. Then the label, in our case describing whether a patient is dyssynchrony or not, is assigned to the nearest class mean.

5.2 Experimental result

The database of 33 studies of MSMP short-axis CMRI is used in our experimental results, with 15 patients labeled as dyssynchronous. However, the database only consist the label on IVD in the LV. Thus, even though we have data on RV, we consider the detection of IVD in LV. To ensure that development of the classifier that distinct two classes, which are the *dyssynchronous* and *non-dyssynchronous* LV, we employ both classes of hearts, and compare and determine the result. In order to classify this database, we first define the RV contours for complete cardiac cycle from our deformable model. Then we apply the classifier to the resulting contours.

The current method of selecting patients for CRT is based on QRS duration on electrocardiography and LV ejection fraction. The eligibility of the CRT using current determination method has an accuracy of 62.5 % [1]. Also, correct classification rate of the database with only LV epicardial and endocardial database of the database is 84.8%. In this project, due to small number of availability in the database, we used the leave-one-out cross validation method, in which we analyzed the 33 classification results from training in the classifier of 32 samples and tested the last sample that was left out. From the database of 33 studies, we have obtained the detection rate of 87.9 % correct classification: this corresponding to misclassifying 4 out of 33 samples. With a slight increase, which is 1 more correct classification out of 33 patients in database, in correct classification, it shows promising improvements in future work which explained in next section.

6. Concluding Remark

We have presented an innovative method of finding and characterizing the ventricular wall motion from the routinely acquired MSMP CMRI sequences. Our main contribution includes the development of the RV tracking deformation model with contour comparison method, and IVD detection from the spatio-temporal shape spaces of the RV.

A semi-automatic deformation model was developed using the complex Fourier shape descriptor parameterization, and used to track RV wall motion over the complete cardiac cycle. The model requires user-supplied initialization on the desired RV boundary of just one image of the CMRI sequence. The model was compared with the manual segmentation contour, and the results indicate that our model is robust to weak contrast, noisy edge map, and irregular motion. From the result, it is found to be that part of the right ventricle interferes with the epicardial boundary of the LV. Figure 3 and Figure 4 shows the non-dyssynchronous and dyssynchronous RV motion. In dyssynchronous RV, dyssynchronous movement of epicardial boundary of the LV seems to be generating dyssynchronous movement in the RV. Since it is much easier to initialize the LV boundary, future work will investigate the deformable model by using the open contour Fourier shape descriptor as shown in Figure 11.

Figure 11: Open Contour Fourier Shape Descriptor Example

We also have developed the technique of detecting the IVD in the LV using RV contour information and only one slice of mid-ventricular CMRI sequence of any cardiac MR system with no additional acquisition techniques. By adopting the statistical pattern recognition technique, we have designed the classifier for IVD detection from the shape descriptor extracted from our deformable model. The results show that the detection of the IVD from shape descriptors extracted from our deformable model is much more accurate than current methods of detection from QRS duration and LV ejection fraction: 87.9 % as compared to 84.8 %, which increase a correct classification by 1 out of 33 patients in the database. Further studies of characterization of IVD as well as improvements of the deformable model are currently being investigated. These include performing segmentation of sets of slices from MSMP short-axis CMRI and long-axis CMRI with larger database. Furthermore, since we have the contour database for the RV, the IVD in the RV as well as bi-ventricular activity (comparing both LV and RV motion) should be investigated. Through these investigations, these structures may improve the characterization of IVD.

References

[1] P. F. U. Gotardo, K. L. Boyer, J. Saltz and S. V. Raman, “A New Deformable Model for Boundary Tracking in Cardiac MRI and Its Application to the Detection of Intra-Ventricular Dyssynchrony,” *Proceedings of the 2006 IEEE Conference on Computer Vision and Pattern Recognition (CVPR 2006), vol. 1, pp. 736-743, New York, June 2006.*

[2] R. N. Fogoros, M.D., “Cardiac resynchronization therapy- CRT,” About Inc 2006 , A part of The New York Times Company, Date observed: March 10, 2006, http://heartdisease.about.com/cs/heartfailure/a/CRT.htm

[3] B.P.F. Leieveldt, R. J. van der Geest, J. H. C. Reiber, “Towards ‘One-Stop’ Cardiac MR image Analysis,” *Imaging Decisions* 2006

[4] V. Chalana and Y. Kim, “A Methodology for Evaluation of Boundary Detection Algorithms on Medical Images” *IEEE Transactions on Medical Imaging*, *Vol. 16, No.5, October 1997*

[5] L. Staib and J. Duncan, “Boundary finding with parametrically deformable models,” *IEEE Transactions on Pattern Analysis and Machine Intelligence*, *vol. 14, no. 11, pp.1061-1075, 1992*

[6] G. Hautvast, S. Lobregt, et al, “Automatic Contour Propagation in Cine cardiac Magnetic Resonance Images” *IEEE Transactions on Medical Imaging*, Vol. 25, No. 11, November 2006

[7] Corsi, C., Gaiani, EG., et al, “Improved Quantification of Right Ventricular Volumes from Cardiac Magnetic Resonance Data,” *IEEE Computers in Cardiology* Vol. 32 pp.37-40, 2005

[8] J. Ivins and J. Porrill, “Everything you always wanted to know about snakes (but were afraid to ask),”*Artificial Intelligence Vision Research Unit,* University of Sheffield, England *Technical Memo* #86, 2000

[9] L. I. Smith, “A tutorial on Principal Components Analysis,” February, 26, 2002, Date viewed January 14, 2007,

http://csnet.otago.ac.nz/cosc453/student_tutorials/principal_components.pdf

[10] M. Welling, "Fisher Linear Discriminant Analysis," Department of Computer Science, University of Toronto, 2006, http://www.cs.huji.ac.il/course/2005/csip/Fisher-LDA.pdf

[11] J.A. Schnurrenberger, "Hierarchical classification and grouping of map spot symbols characterized by Fourier descriptors," Master's thesis, Graduate School of The Ohio State University, Columbus, OH, 1998